

Three-dimensional digital beamforming for near-field wideband acoustic imaging

Maria Palmese, Andrea Trucco, Gianni Vernazza
Department of Biophysical and Electronic Engineering (DIBE)
University of Genoa

Via all'Opera Pia 11, I - 16145 Genova (Italy).
Phone: +39 010 353 2015 (Trucco); E-mail: trucco@dibe.unige.it

Abstract. *To generate volumetric acoustic images, a planar array of sensors is required to collect the signals coming from a 3-D scene. The method most frequently used to process the acquired signals is a digital beamforming algorithm. In general, due to the high number of sensors and beam signals, the computational load is prohibitive for real-time image generation. In this paper, the options for a frequency-domain implementation are discussed and an extension of the Chirp Zeta Transform beamforming is proposed that has been specifically devised to cope with the requirements of volumetric imaging. In particular, the process of wideband signals collected by a planar array and generated by a scene placed in both the near-field and the far-field is enabled with a computational load that is a few orders of magnitude lower than that of the traditional frequency-domain and time-domain beamforming implementations.*

I. INTRODUCTION

Despite the introduction of commercial equipment, building systems able to generate a real-time 3-D acoustic video of an investigated environment [1,2] is still a challenge, mainly due to the cost of the needed planar array and the computational load associated with the digital beamforming technique [1]. Moreover, 3-D imaging systems should be able to work in the near-field region, imposing a focused beamforming approach [1-3], and this causes additional difficulties, especially when beamforming is implemented in the frequency domain. To overcome problems related to hardware costs and computational load, several options have been pursued in recent decades and are still the focus of investigation. Among these options, the possibility of avoiding digital beamforming by using acoustic lenses is particularly attractive, as described and reviewed in [4]. Although results of high quality have been obtained for specific set-ups, the limited efficiency of acoustic lenses and the poor flexibility of the systems based on them, especially in the near-field region, still inhibit the widespread adoption of this technique. Another interesting option to limit the computational flux and the hardware costs is the

synthetic aperture strategy [5,6], which can be applied to the 3-D imaging case with different techniques [7,8]. However, the need to transmit a sequence of pulses often does not allow one to obtain real-time imaging or to deal with moving objects, especially in underwater contexts, where the pulse repetition rate is limited by the maximum range of the system, which can exceed several meters.

The computational burden and the hardware requirements of digital beamforming implemented in the time-domain can be mitigated by using one of the approximate implementations [9-11] proposed in recent years or by adopting a sparse planar array of sensors [12]. In both cases, a loss of quality is an unavoidable consequence and, given the purpose of the imaging systems, unacceptable. Even the use of specific integrated circuits based on proprietary technologies [13] to perform the time-domain beamforming is a solution with limited flexibility that is rarely acceptable.

Beamforming implementation in the frequency domain represents an attractive alternative that has been extensively investigated [3,14,15] in an attempt to exploit the computational advantages of the fast Fourier transform (FFT). In [15], Maranda thoroughly described and compared some frequency-domain beamforming methods, with reference to a one-dimensional (1-D) array and a far-field condition. He divided these into exact and approximate methods.

Traditionally, “direct method” (DM) beamforming is the most widely applied of the exact methods, and its extension to planar arrays and near-field conditions has been introduced and extensively investigated [16,17]. The computational load of the frequency-domain DM is significantly lower than that of time-domain beamforming, and its efficient implementation on digital computation platforms can represent an additional advantage.

Zero-padded FFT beamforming is the most widely applied of the approximate methods, and its extension to planar arrays has been investigated [18,19], also with reference to the near-field condition. This method is very efficient and exact for narrowband signals [18]. However, the extension to wideband signals is not straightforward and introduces errors: the computational load is much greater if major errors are to be avoided, thus decreasing the expediency of the method [15].

Although less recognized, Chirp Zeta Transform (CZT) beamforming [15] is a flexible frequency-domain method that can process wideband signals without any error, with a computational load equal to or lower than that of zero-padded FFT beamforming. In [15], with reference to 1-D arrays and far-field conditions, Maranda judged CZT beamforming to be better than the “direct method” and the zero-padded FFT algorithms. Recently, the extension of CZT beamforming to planar arrays and far-field conditions has been introduced [20] and assessed, with the same conclusions that Maranda sketched for 1-D arrays.

In this paper, an original beamforming technique for wideband 3-D imaging is proposed, based on CZT beamforming that has been specifically tailored to image a volume of space encompassing the near-field and far-field regions, with a convenient computational load. The near-field difficulties have been solved by the adoption of the Fresnel approximation [1,3,18] for the beamforming delays, a useful definition of the steering angles, and the setting of multiple focal regions. In addition, a technique to generate cubic resolution cells has also been introduced, allowing a further reduction of the computational burden. The resulting computational load is evaluated and compared with those of different frequency-domain and time-domain techniques, showing that the devised solution offers noticeable computational advantages. Moreover, except for the Fresnel approximation (whose validity region is discussed later), the frequency-domain digital beamforming proposed here should be considered an exact method.

On the whole, this paper introduces an innovative digital method for 3-D acoustical imaging that is computationally advantageous and suitably flexible for real operations. Although the application context assumed in this paper refers to underwater sonar systems, the proposed technique can also be positively exploited for medical or non-destructive testing applications.

II. PLANAR ARRAYS AND NEAR-FIELD CONDITIONS

Let us consider a planar array placed on the plane xy , composed of $M \times N$ sensors. The sensor identified by the indexes (m, n) is placed at position (x_m, y_n) and generates the signal $s_{m,n}(t)$. The steering direction is identified by a couple of azimuth and elevation angles (θ_a, θ_e) that, in contrast to the conventional formalism [2,18], are defined as shown in Fig. 1. The choice of such angles is useful for easily extending CZT beamforming to a planar array. Although the conventional formalism also makes it possible to express the main computation as a discrete convolution, it is less direct and intuitive.

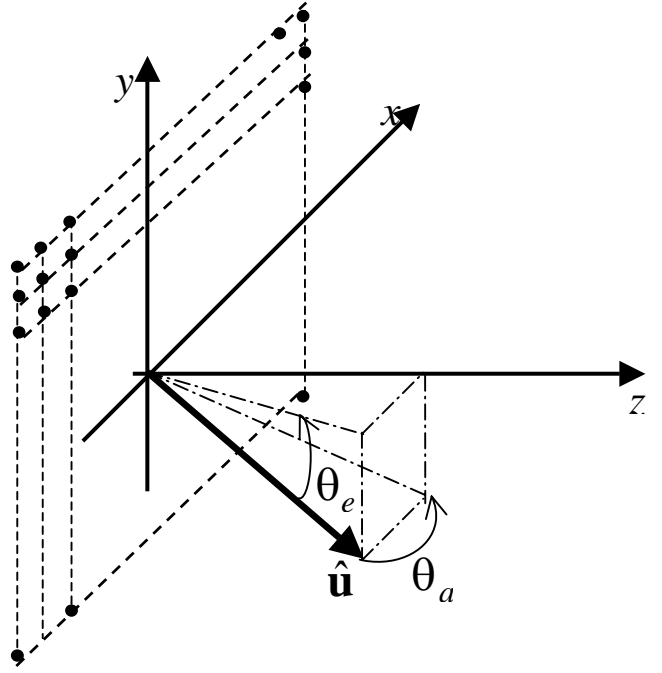


Figure 1. Notation and geometry for a planar array.

According to such a notation, the unit vector of the steering direction, $\hat{\mathbf{u}}$, can be expressed as:

$$\hat{\mathbf{u}} = \left[\sin\theta_a, \sin\theta_e, \sqrt{\cos^2\theta_a - \sin^2\theta_e} \right]$$

where θ_a is the angle between the vector $\hat{\mathbf{u}}$ and its projection on the plane yz , and θ_e is the angle between the vector $\hat{\mathbf{u}}$ and its projection on the plane xz .

According to delay-and-sum beamforming [1], if the far-field condition is still valid, the beam signal, $b(t, \theta_a, \theta_e)$, steered in the direction (θ_a, θ_e) , can be expressed as follows:

$$b(t, \theta_a, \theta_e) = \sum_{m=0}^{M-1} \sum_{n=0}^{N-1} w_{m,n} s_{m,n} \left(t - \frac{x_m \sin\theta_a + y_n \sin\theta_e}{c} \right)$$

where $w_{m,n}$ is the apodizing weight assigned to the (m,n) -sensor. The extension of the CZT beamforming to an equispaced planar array working in far-field conditions has been introduced by the authors in [20].

This paper focuses on near-field conditions, where the curvature of the wavefront cannot be neglected, and a focusing distance r_0 should be introduced in the delay term [1,3,18], which, in turn, becomes much more complex. The last equation (delay-and-sum beamforming) is modified as follows:

$$b(t, \theta_a, \theta_e, r_0) = \sum_{m=0}^{M-1} \sum_{n=0}^{N-1} w_{m,n} s_{m,n} \left(t - \tau_{m,n}(\theta_a, \theta_e, r_0) \right)$$

$$\tau_{m,n}(\theta_a, \theta_e, r_0) = \frac{r_0 - \sqrt{r_0^2 + x_m^2 + y_n^2 - 2x_m \sin \theta_a - 2y_n \sin \theta_e}}{c}$$

The computation of the delay terms given in the last equation is computationally very heavy; therefore, it is necessary to compute and store them a priori. The number of possible combinations among m , n , θ_a , θ_e , and r_0 requires a very large memory. To simplify such a delay and reduce the memory needs, the Fresnel approximation can be applied [1,3,18], obtaining the following term:

$$\tau_{m,n}(\theta_a, \theta_e, r_0) = \frac{x_m \sin \theta_a}{c} + \frac{y_n \sin \theta_e}{c} - \frac{x_m^2 + y_n^2}{2r_0 c}$$

The validity region of the Fresnel approximation (i.e., the region where the approximation errors are negligible) is discussed by Ziomek [18].

The beamforming implementation in the frequency domain requires the temporal sampling of the signals gathered by the sensors, producing the time series $s_{m,n}(l)$, followed by the segmentation into partially overlapped blocks of length K and the transformation into their frequency versions, $S_{m,n}(k)$, by the FFT. If the Fresnel approximation is adopted, the DFT coefficients $B(k, \theta_a, \theta_e, r_0)$ of the beam signal $b(t, \theta_a, \theta_e, r_0)$ are given by the following expression:

$$B(k, \theta_a, \theta_e, r_0) = \sum_{m=0}^{M-1} \sum_{n=0}^{N-1} \left\{ w_{m,n} \exp \left(j2\pi f_k \left(\frac{x_m^2 + y_n^2}{2r_0 c} \right) \right) S_{m,n}(k) \cdot \exp \left(-j2\pi f_k \left(\frac{x_m \sin \theta_a}{c} + \frac{y_n \sin \theta_e}{c} \right) \right) \right\}$$

which represents the DM for a near-field, frequency-domain beamforming.

Let us assume now that the planar array placed on the plane xy is centered on the coordinate origin and equispaced, with an intersensor spacing d in both directions. Let us consider the computation of a pyramid of beams composed of $M_b \times N_b$ signals, identified by the indexes (p, q) . For each of these beams, the steering direction is $(\theta_{a,p}, \theta_{e,q})$, where $\theta_{a,p}$ and $\theta_{e,q}$ are two angles chosen from a set of M_b azimuth angles and a set of N_b elevation angles, respectively. The predefined angles are equispaced in the sine domain, ranging from an initial to a final angle. After some mathematics, the k -th Fourier coefficient of the beam signal (p, q) , focused at a distance r_0 , can be written as follows:

$$B(k, \theta_{a,p}, \theta_{e,q}, r_0) = W_a^{\frac{-p^2}{2}} W_e^{\frac{-q^2}{2}} \sum_{m=0}^{M-1} \sum_{n=0}^{N-1} \left\{ v_{m,n} S_{m,n}(k) A_a^m A_e^n W_a^{\frac{-m^2}{2}} W_e^{\frac{-n^2}{2}} \cdot \frac{-n^2}{W_e^2} \frac{(p-m)^2}{W_a^2} \frac{(q-n)^2}{W_e^2} \right\}$$

The terms W_a , A_a , W_e , and A_e , are defined as follows:

$$A_a = \exp \left(-j2\pi f_k \frac{d}{c} \sin \theta_{ai} \right)$$

$$W_a = \exp \left(j2\pi f_k \frac{d}{c} \Delta s_a \right)$$

$$A_e = \exp \left(-j2\pi f_k \frac{d}{c} \sin \theta_{ei} \right)$$

$$W_e = \exp \left(j2\pi f_k \frac{d}{c} \Delta s_e \right)$$

where:

$$\Delta s_a = \frac{\sin \theta_{af} - \sin \theta_{ai}}{M_b - 1},$$

$$\Delta s_e = \frac{\sin \theta_{ef} - \sin \theta_{ei}}{N_b - 1},$$

θ_{ai} and θ_{af} are the initial and final steering angles for the azimuth, respectively, and θ_{ei} and θ_{ef} are the initial and final steering angles for the elevation, respectively. The steering angles $\theta_{a,p}$ and $\theta_{e,q}$ can be derived from the following relations:

$$\sin \theta_{a,p} = \sin \theta_{ai} + \Delta s_a p, \quad p = 0, \dots, M_b - 1$$

$$\sin \theta_{e,q} = \sin \theta_{ei} + \Delta s_e q, \quad q = 0, \dots, N_b - 1$$

The term $v_{m,n}$ is defined as follows:

$$v_{m,n} = w_{m,n} \exp \left\{ j2\pi f_k \left[\left(m - \frac{M-1}{2} \right)^2 + \left(n - \frac{N-1}{2} \right)^2 \right] \frac{d^2}{2r_0 c} \right\}$$

A previous equation expresses $B(k, \theta_{a,p}, \theta_{e,q}, r_0)$ as a 2-D discrete convolution of the following two matrixes $\mathbf{C}(k)$ and $\mathbf{D}(k)$:

$$\mathbf{C}(k) = v_{m,n} S_{m,n}(k) A_a^m A_e^n W_a^{\frac{-m^2}{2}} W_e^{\frac{-n^2}{2}}$$

$$\mathbf{D}(k) = W_a^{\frac{m^2}{2}} W_e^{\frac{n^2}{2}}$$

where $n \in [0, N-1]$ and $m \in [0, M-1]$, thereby allowing FFT methods for performing the 2-D ‘‘fast convolution’’ [21] to be used effectively. It is worth noting that, at a single frequency f_k , the convolution FFT-based method simultaneously computes all the values of the $M_b \times N_b$ beams. Finally, after all the segments of the beams are computed over the desired frequency band, $M_b \times N_b$ inverse FFTs are necessary to obtain the beam time series.

III. DEPTH OF FIELD AND RANGE RESOLUTION

In this Section, two solutions intended to optimize the computational load while preserving the imaging system performance are proposed. The first one concerns the length K of the signal blocks in relation to the depth of field and the focal regions to be defined. The second one is related to the number of frequency bins to be processed in relation to the range resolution. It will be shown that a dynamic tuning of both the block length and the number of bins with the distance is convenient. The two solutions can be applied to both DM and CZT frequency-domain beamforming.

In near-field beamforming (independently on the time or frequency implementation), the depth of field (DOF) is the range interval around the focusing distance r_0 inside which the performances only marginally degrade. More precisely, often the DOF is determined by examining the array beam pattern versus the distance r in the steering direction. The points r_{0-} and r_{0+} , where a reduction of 3 dB with respect to the beam-pattern maximum (i.e., the value in r_0) occurs, are defined as the DOF limits [2, 22]. The extension of the DOF (i.e., $r_{0+} - r_{0-}$) depends on the specific value of r_0 : the smaller the focusing distance r_0 , the smaller the DOF extension.

For a square array with a side length D , the near-field limit is placed at a distance, r_{nf} , defined as follows:

$$r_{nf} = \frac{D^2}{2\lambda}$$

where λ is the wavelength of the central frequency of the acoustic pulse spectrum. For $r_0 < r_{nf}$, assuming that the central element of the array is chosen as the centre of phase, the DOF limits can be computed by the following, approximated, closed-form expressions:

$$r_{0-} = r_0 - \frac{r_0}{\left(D^2 / 2\lambda r_0\right) + 1}$$

$$r_{0+} = r_0 + \frac{r_0}{\left(D^2 / 2\lambda r_0\right) - 1}$$

In 3-D acoustic imaging for underwater applications, the range extension of the volume to be imaged is in general very large: part of it is placed inside the near-field region, the remaining part is placed inside the far-field region. The part in the far-field does not require any focusing [20]. The part in the near-field requires beamforming focusing, but it often has an extension that exceeds that of the DOF. The problem is commonly solved by segmenting the received time signals into subsequent blocks that are processed using different focusing distances r_0 that increase with time. In

other words, the part of the volume to be imaged that is placed inside the near-field region is subdivided into multiple, adjacent focal regions. Each focal region is referred to a specific focusing distance r_0 and is contained inside the DOF corresponding to such a focusing distance. As in the frequency-domain beamforming (both the direct method and the CZT method) the time signals are segmented into blocks of length K , one can easily apply different focusing distances to each block coming from the near-field region.

However, in assigning a value to K , two opposing requirements should be considered: (1) the spatial extension corresponding to K time samples should not exceed the shortest among the extensions of the focal regions (the extension of the focal region closest to the array). This requirement implies a small value for K . (2) For a given imaging system, there is an optimum value of K in terms of computational burden. Typically, this value is larger than the smallest focal region. To satisfy both the requirements, a dynamic block length assignment can be adopted, allowing the length of the signal blocks to vary, increasing in synchrony with the DOF extension until the optimum K value is reached.

The second solution proposed in this Section can be referred to as dynamic range resolution. The angular resolution of the beamforming system is constant; as a consequence, the lateral resolution worsens with the distance. On the contrary, the range resolution depends on the pulse bandwidth and does not vary with the distance. The objective of a volumetric imaging system is generally that to produce cubic resolution cells [1]: in this light, a worsening of the range resolution with the distance, in synchrony with the worsening of the lateral resolution, would be perfectly acceptable. This makes it possible to save many operations by reducing the number of frequency bins processed (i.e., the bandwidth considered) with the distance r . Recalling that the range resolution is $c / (2Q)$, with Q being the bandwidth of the pulse and assuming a uniform array weighting where the lateral resolution is $0.88\lambda r / (Nd)$, one can conclude that the bandwidth necessary to make equal the two resolutions, at a given distance r , is the following:

$$Q = \frac{c N d}{1.76 \lambda r}$$

If the weighting is not uniform, the lateral resolution worsens a little, the necessary bandwidth Q decreases, and the computational load is, in turn, slightly reduced. Therefore, for a given block of the time signals, denoting with r^* the distance at which the block starts, the number of frequency bins, ζ , to be considered in order to achieve a range resolution not worse than the lateral resolution is the following:

$$\zeta = \text{ceil} \left(\frac{c K N d}{1.76 f_s \lambda r^*} \right)$$

where K is the length of the signal block, f_s is the sampling frequency, and the function $\text{ceil}(a)$ rounds a to the nearest integer towards infinity.

In this way, the generation of cubic resolution cells is enabled, and the number of operations involved in the beam computation is drastically reduced, because the equation for $B(k, \theta_a, p, \theta_e, q, r_0)$ should be evaluated for a number of indexes k that decreases block after block, according to ζ .

IV. COMPARISON AND DISCUSSION

The aim of this Section is to compute the total number of operations needed to generate a whole 3-D image and to compare the computational loads of the three beamforming techniques considered. To make it possible such a comparison, it is necessary to set some of the variables that influence the computational burden. With reference to an underwater imaging application, some of them are fixed as follows: sound speed, $c = 1500$ m/s; central frequency of the acoustic pulse, 500 kHz; pulse bandwidth, 250 kHz; sampling frequency of the time signals, $f_s = 1.5$ MHz; intersensor spacing in both directions, $d = \lambda/2 = 1.5$ mm; range extension of the volume to be imaged from 1 m to 50 m. For the time-domain beamforming an interpolating filter with $H = 100$ stages is assumed [3]. The analysis of the computational load is carried out with respect to: the number of sensors along the array side, N ; the number of beams along the pyramid side, N_b ; and the length of the signal blocks, K .

For both the frequency-domain implementations (i.e., DM and CZT), the two solutions described previously (i.e., dynamic range resolution and dynamic block length assignment) have been assumed enabled in the evaluation of the computational burden.

A first analysis concerns the impact on the computational burden of the value K at which the maximum block length is set. Assuming the ratio N_b/N equal to 2, the number of real operations required by the CZT and the DM beamforming techniques, as a function of the array lateral size N , to create one 3-D image is shown in Figs. 2(a) and 2(b), respectively. The two panels compare four different values of K , showing that for values higher than 512 the number of operations is almost independent on K . Instead, for $K = 512$, the overlapping among successive blocks causes a significant increment of the number of operations, especially if the lateral size of the array exceeds $N = 100$. These considerations are valid for both CZT and DM beamforming, although the total operation count of the DM case is over one order of magnitude higher than that of the CZT case. In the following of this paper, K will be set equal to 2048; more in general, the value of K can be profitably set according to the hardware features.

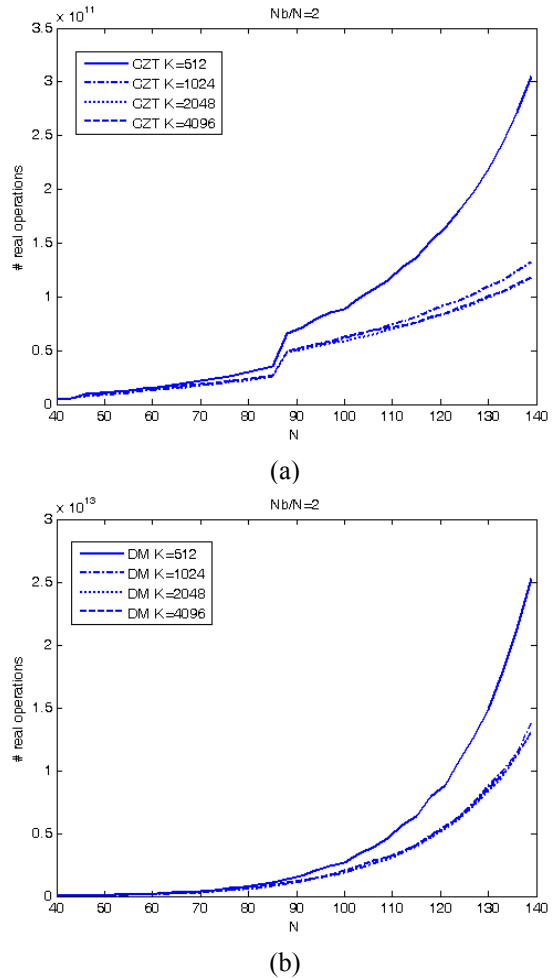


Figure 2. Operation count versus the array lateral size N , for different values of the block length K . $N_b/N = 2$. (a) CZT beamforming. (b) DM beamforming.

Setting $K = 2048$ and $N_b/N = 2$, the computational load of the three beamforming technique to create one 3-D image is compared, as a function of the array lateral size N , in Fig. 3. The graphs reveal that the CZT beamforming is very convenient with respect to D&S and DM beamforming techniques. With respect to D&S, there is an approximately 10-fold advantage when N is 40, which increases to 1000 when N is 140. Even more efficient than D&S, DM is more computationally demanding than CZT: the 4-fold advantage of CZT when N is 40 increases to 100 when N is 140. Therefore, CZT beamforming becomes more and more attractive when the size of the planar array increases, providing a very important gain. In fact, under the hypothesized conditions, the time-domain D&S method and the frequency-domain DM present a steeper rise of operations along with the array size increase.

Also the impact of the ratio N_b/N on the computational load of the three beamforming techniques is analyzed in Fig. 4. The results shown in Fig. 4 have

been obtained with $K = 2048$ and $N = 80$. The operation counts of D&S and DM beamforming gradually increase with N_b . Instead, the CZT-based technique shows an operation count almost constant, with a step at $N_b/N = 2.2$. The reason is twofold: (1) The computational load of the spatial processing is constant for all the values of $N + N_b - 1$ included between two contiguous powers of two. (2) The computational load of the inverse FFT increases with N_b . However, the increase is negligible with respect to the total operation count.

CZT beamforming is still dramatically advantageous, reporting an approximately 10-fold gain as compared to DM at $N_b = 80$ and about 25-fold at $N_b = 120$, and achieving a 100-fold gain with respect to D&S at $N_b = 80$ and 750-fold at $N_b = 120$.

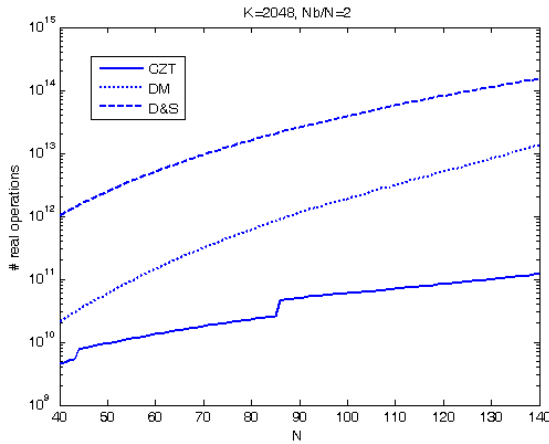


Figure 3. Operation count for the three beamforming methods (i.e., CZT, DM, D&S) as a function of the array lateral size N . $K = 2048$ and $N_b/N = 2$.

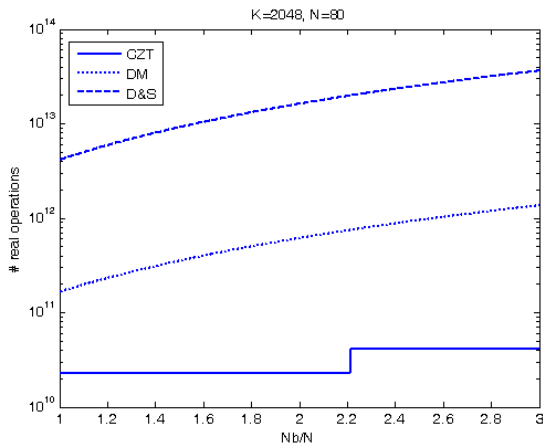
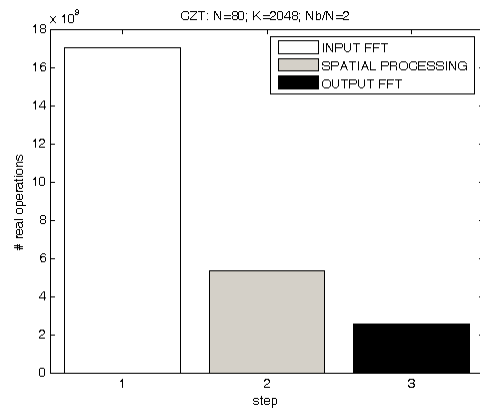
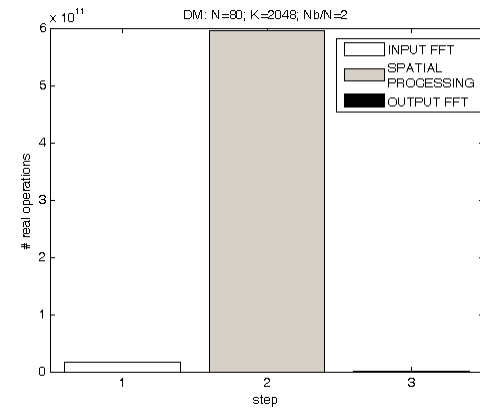


Figure 4. Operation count for the three beamforming methods (i.e., CZT, DM, D&S) as a function of the ratio N_b/N . $K = 2048$ and $N = 80$.

An analysis of the computational weight of the three steps (i.e., the FFT of the input signals, the spatial processing, and the inverse FFT of the output beam signals) needed to produce a volumetric image, using CZT beamforming and DM beamforming, is shown in Fig. 5. The diagrams refer to the case: $K = 2048$, $N = 80$, and $N_b/N = 2$. The first and the third steps (input and output FFT) involve a number of operations that do not depend on the beamforming technique; consequently, their computational load is equal for CZT and DM beamforming. (Unfortunately, the different scales used in Figs. 5(a) and 5(b) make it difficult to verify this fact.) On the contrary, the second step (spatial processing) of DM beamforming requires a number of operations that is approximately 100-fold higher than that required by CZT beamforming. Apart from this advantage, it is interesting to note that, for CZT beamforming, the heaviest processing step is the FFT of the input signals. This observation can guide to set the type and the characteristics and of the hardware to be used.



(a)



(b)

Figure 5. Analysis of the computational load of the three processing steps for the generation of a volumetric image. (a) CZT beamforming. (b) DM beamforming. $N = 80$, $K = 2048$, and $N_b/N = 2$.

Overall, one can note that, for the system considered, the CZT beamforming reports a computational advantage of about one order of magnitude with respect to the DM beamforming, and of about two orders of magnitude with respect to D&S beamforming.

Finally, a comment on the Fresnel approximation of the beamforming delays to be applied in the near-field region is useful. While the D&S and DM beamforming techniques can be implemented using the exact delays or the approximated delays (the choice depending on the size of the available memory, with no impact on the on-line computational load), the CZT beamforming needs the use of the approximated delays. Although this can appear as a drawback, it is important to remark that the computed beam signals do not present any significant inaccuracy provided that they are pointed and focused inside the validity region [18] of such an approximation. For this reason the Fresnel approximation is well known and widely adopted. In addition, a method to enlarge the validity region of such an approximation, according to the angular extension of the imaged region, has been proposed in [23] and can be applied to the CZT beamforming without any increase in the computational burden.

V. CONCLUSIONS

This work focused on extending the CZT beamforming method to the case of a planar array for 3-D near-field digital beamforming. Although CZT beamforming is carried out in the frequency domain, it overcomes the typical problems affecting other frequency beamforming techniques, such as zero-padded FFT beamforming. In particular, the samples of the beam signals computed for every frequency bin are related to the same set of predefined steering angles. Moreover, the initial and final angles of the scanned sector can be arbitrarily selected. The Fresnel approximation in the delay computation and the setting of multiple focal regions was necessary to extend CZT to the near-field case. An adequate organization of the different operations and the introduction of a technique to generate cubic resolution cells have allowed one to reduce the number of online operations necessary to generate a 3-D image dramatically. The computational analysis has shown that the advantage of CZT beamforming with respect to D&S time-domain beamforming and to DM frequency-domain beamforming is important, especially when the later size of the planar array increases. For a realistic set-up of an underwater volumetric imaging system, the gain factor obtained with CZT beamforming is larger by over one order of magnitude compared to DM beamforming, and increases to over two orders of magnitude compared to D&S beamforming.

ACKNOWLEDGMENTS

Special thanks to PARVIS Systems and Services, Milan, Italy, for its generous financial support.

REFERENCES

- [1] V. Murino and A. Trucco, "Three-Dimensional Image Generation and Processing in Underwater Acoustic Vision," *Proceedings of the IEEE*, vol. 88, pp. 1903-1946, 2000.
- [2] T.L. Szabo, *Diagnostic Ultrasound Imaging: Inside Out*, Elsevier Academic Press, Amsterdam, 2004.
- [3] R.O. Nielsen, *Sonar Signal Processing*, Artech House, Boston, 1991.
- [4] I. Kaiho, "A dream for realization of high-speed, 3D volume image by lens-focused method," *Proc. 7th Cong. Asian Fed. Ultrasound Med. Biol.*, International Congress Series Elsevier, vol. 1274, pp. 38-46, 2004.
- [5] J.A. Jensen, S.I. Nikolov, K.L. Gammelmark, M.H. Pedersen, "Synthetic aperture ultrasound imaging," *Ultrasonics*, vol. 44, sup. 1, pp. e5-e15, 2006.
- [6] J.A. Johnson, M. Karaman, B.T. Khuri-Yakub, "Coherent-array imaging using phased subarrays. Part I: basic principles", *IEEE Trans. Ultrasonics, Ferroelectrics, and Frequency Control*, vol. 52, pp. 37-48, 2005.
- [7] N.M. Daher and J.T. Yen, "2-D array for 3-D ultrasound imaging using aperture techniques", *IEEE Trans. Ultrasonics, Ferroelectrics, and Frequency Control*, vol. 53, pp. 912-924, 2006.
- [8] J.A. Johnson, M. Karaman, B.T. Khuri-Yakub, "Phased Subarray Processing for underwater 3D acoustic imaging," *MTS/IEEE Oceans 2002*, Biloxi, Mississippi, pp. 2145-2151, 2002.
- [9] V. Murino, C.S. Regazzoni, A. Trucco, and G. Vernazza, "A Non-Coherent Correlation Technique and Focused Beamforming for Ultrasonic Underwater Imaging: a Comparative Analysis", *IEEE Trans. Ultrasonics, Ferroelectrics, and Frequency Control*, vol. 41, pp. 621-630, 1994.
- [10] K. Ranganathan, M.K. Santy, T.N. Blalock, J.A. Hossack, W.F. Walker, "Direct Sampled I/Q Beamforming for Compact and Very Low-Cost Ultrasound Imaging", *IEEE Trans. Ultrasonics, Ferroelectrics, and Frequency Control*, vol. 51, pp. 1082-1093, 2004.
- [11] A. Agarwal, Y.M. Yoo, F.K. Schneider, C. Gao, L.M. Koh, Y. Kim, "New Demodulation Method for Efficient Phase-Rotation-Based Beamforming," *IEEE Trans. Ultrasonics, Ferroelectrics, and Frequency Control*, vol. 54, pp. 1656-1667, 2007.
- [12] A. Trucco, M. Palmese, S. Repetto "Devising an Affordable Sonar System for Underwater 3-D Vision", *IEEE Trans. Instrument. and Measurement*, vol. 57, pp. 2348-2354, 2008.
- [13] A. Chiang, S.R. Broadstone, J.M. Impagliazzo, "A low Power Imaging and Obstacle Avoidance Sonar for Small UUVs", *Int. Conf. Oceans 2003 MTS/IEEE*, San Diego, California (USA), pp. 1875-1881, 2003.

- [14] R.A. Mucci, "A Comparison of Efficient Beamforming Algorithms," *IEEE Trans. Acoust., Spec., Signal Proc.*, vol. ASSP-32, pp. 548-558, 1984.
- [15] B. Maranda, "Efficient Digital Beamforming in the Frequency Domain," *Journal of Acoustical Society of America*, vol. 86, pp. 1813-1819, 1989.
- [16] F. Zhang, A. Bilas, A. Dhanantwari, K.N. Plataniotis, R. Abiprojo, and S. Stergiopoulos, "Parallelization and Performances of 3D Ultrasound Imaging Beamforming Algorithms on Modern Clusters", *Proc. of the 16th ACM Int. Conf. on Supercomputing*, New York (USA), 2002.
- [17] A.C. Dhanantwari, S. Stergiopoulos, L. Song, C. Parodi, F. Bertora, P. Pellegritti. A. Questa, "An efficient 3D beamformer implementation for real-time 4D ultrasound systems deploying array probes", *2004 IEEE Ultrasonics Symposium*, Toronto, Ontario (Canada), pp. 1421-1424, 2004.
- [18] L.J. Ziomek, *Fundamentals of Acoustic Field Theory and Space-Time Signal Processing*, CRC Press, Boca Raton, Florida (USA), 1995.
- [19] V. Murino, A. Trucco, "Dynamic Focusing by FFT Beamforming for Underwater 3D Imaging", *Acoustics Letters*, vol. 17, pp. 169-172, 1994.
- [20] M. Palmese, A. Trucco, "3-D Acoustic Imaging by Chirp Zeta Transform Digital Beamforming," *IEEE Trans. Instrument. and Measurement*, vol. 57, 2009 (in press).
- [21] A.V. Oppenheim, R.W. Schaffer, *Digital Signal Processing*, Prentice-Hall, Englewood Cliffs, NJ (USA), 1973.
- [22] R.C. Hansen, "Focal Region Characteristics of Focused Array Antennas," *IEEE Trans. on Antennas and Propagation*, vol. AP-33, pp. 1328-1337, 1985.
- [23] A. Trucco, "A Least-Squares Approximation for the Delays Used in Focused Beamforming," *Journal of Acoustical Society of America*, vol. 104, pp. 171-175, 1998.